



# Model for Ruhrstahl–Heraeus (RH) decarburization process

Dong-ping Zhan<sup>1,2</sup> · Yang-peng Zhang<sup>3</sup> · Zhou-hua Jiang<sup>1</sup> · Hui-shu Zhang<sup>4</sup>

Received: 5 March 2017 / Revised: 11 July 2017 / Accepted: 21 July 2017 / Published online: 17 April 2018  
© China Iron and Steel Research Institute Group 2018

## Abstract

A mathematical model was established to predict the carbon content of ultralow carbon steel in the Ruhrstahl–Heraeus (RH) process. The model was solved using the fourth-order Runge–Kutta method and assumed that the volume of steel partaking in the reaction depends on the decarburization mechanism. After analyzing the decarburization process using the proposed model, the following conclusions were drawn. First, the initial carbon and oxygen contents in the RH degasser should be stabilized in the range of  $(200–350) \times 10^{-6}$  and  $(500–700) \times 10^{-6}$ , respectively. Second, in the initial stage, the pressure should be reduced as quickly as possible. Third, oxygen blowing should begin as early as possible when the forced decarburization is needed and the minimum oxygen flow rate should be  $0.1923 \text{ m}^3/(\text{t min})$ . Finally, expanding the diameter of the snorkel tube from 480 to 600 mm clearly enhances the decarburization rate.

**Keywords** RH · Model · Carbon content · Fourth-order Runge–Kutta · Ultralow carbon steel · Decarburization

## 1 Introduction

The Ruhrstahl–Heraeus (RH) degasser is the most widely used vacuum decarburization unit in secondary steelmaking processes, including the production of ultralow carbon steel [1–4]. The RH degasser exerts an effective vacuum- and argon-stirring effect and provides good dynamic conditions for decarburization. Moreover, the top-blow oxygen lance can increase the oxygen content to deal with different situations.

Currently, the utility of the RH degasser in the production of ultralow carbon steel is limited by the long treatment time. This problem is linked to the operating process and end point, which the operator cannot easily judge from the condition of the equipment and the carbon content in the

molten steel. Therefore, developing a process that accurately calculates carbon content has become a focus of modern research on ultralow carbon steel production. Previous studies have modeled the behavior of the decarburization process from a variety of perspectives [5–19].

Yamaguchi et al. [5] assumed that molten steel exhibited ideal flow behavior. They divided molten steel into two compartments: the vacuum vessel (the main site of the decarburization reaction) and the ladle; then, they proposed a model based on the carbon–oxygen balance and solved its equations using a fourth-order Runge–Kutta (R–K) method. Takahashi et al. [6] established a model based on the decarburization mechanism. Their model proposed three sites for the decarburization reaction: the surfaces of Ar bubbles, CO bubbles produced via the carbon–oxygen reaction, and surface of the molten steel in the vacuum vessel. This model considered the different carbon contents in the vacuum vessel and ladle. Because it ignored liquid steel turbulence, this type of calculation rapidly converged; however, it also delivered high precision and had therefore rapidly become accepted worldwide [5–9, 13–16, 18]. Saint-Raymond et al. [9] calculated the amount of decarburization in different parts (CO bubbles, splash droplet surfaces, and Ar bubble surfaces) and proposed a decarburization mechanism model based on mass balance. Later, Van Ende et al. [15] established a molten steel, gas, and slag equilibrium model based on the FACT database (a

✉ Dong-ping Zhan  
zhandp1906@163.com

<sup>1</sup> School of Metallurgy, Northeastern University, Shenyang 110819, Liaoning, China

<sup>2</sup> Shenyang Northeastern Institute of Metal Materials Co., Ltd., Shenyang 110108, Liaoning, China

<sup>3</sup> School of Materials Science and Engineering, Northeastern University, Shenyang 110819, Liaoning, China

<sup>4</sup> Metallurgical Engineering College, Liaoning Institute of Science and Technology, Benxi 117004, Liaoning, China

thermochemical database that is widely used by metallurgists).

An alternative approach for analyzing the behavior of the decarburization process is the finite element model. This approach accounts for the flow field and the maldistribution of the carbon content in molten steel [10–12, 14, 15, 17, 19]. A more complex model, GENGDIANQIAO [19], coupled the flow field and distribution of inclusions with the decarburization process. Although this type of model accurately calculates the carbon content at different locations, it incurs a huge computational cost and is not conducive to engineering applications.

Currently, most of the models used in engineering applications adopt Saint-Raymond's approach [9]. In this approach, first, the vacuum vessel and ladle are separated as two areas. The vacuum area is reserved mainly for decarburization, while the ladle area is designated as a high carbon molten steel supply area. Next, the amount of carbon removed from various sites (CO bubbles, splash droplet surfaces, Ar bubble surfaces, and the free surface in the vacuum vessel) is calculated. Finally, these calculations are integrated into a mass balance model.

However, these models assume that the weight of the molten steel partaking in the reaction at different sites is the weight of molten steel in the vacuum vessel; this assumption is inconsistent with the facts [5–9, 13–16, 18]. Therefore, an alternative decarburization model that does not compartmentalize molten steel but instead calculates the molten steel weight at different reaction sites and sums the amounts of carbon removed at different sites to obtain the total carbon removal is established. The model is solved by the fourth-order R–K method.

## 2 Mathematical model

### 2.1 Mechanism of RH decarburization

The decarburization reaction proceeds according to the following equation:  $[C] + [O] = CO(g)$ . The equilibrium constant  $K$  of this reaction is calculated as follows [16]:

$$K = \frac{P_{CO}^*}{a_C a_O} \approx \frac{P_{CO}^*}{w_C w_O} = 10^{1160/T+2.003} \quad (1)$$

where  $P_{CO}^*$  is the partial pressure of CO in gas phase, Pa;  $a_C$ ,  $a_O$  are the activities of C and O, respectively, in molten steel;  $w_C$ ,  $w_O$  are the mass fractions of C and O, respectively, in molten steel; and  $T$  is temperature of molten steel, K.

### 2.2 Assumption and model

In the proposed mathematical model of natural RH decarburization, decarburization occurs at three sites: the interior

of molten steel, free surface of the argon gas, and surfaces of the splash droplets. Moreover, the following assumptions are made.

- (1) The carbon and oxygen concentrations at the gas–metal interface equilibrate with the partial pressure of CO in the gas phase.
- (2) Molten steel is perfectly mixed in the ladle.
- (3) The decarburization rate is controlled by the chemical reaction at gas–metal interface between carbon and oxygen.

Under these assumptions, the mass balances of carbon and oxygen in the vessel are given, respectively, by

$$W \frac{dC_C}{dt} = W_{CO} \times \frac{dC_{CO}}{dt} + W_{Ar} \times \frac{dC_{Ar}}{dt} + W_{Splash} \times \frac{dC_{Splash}}{dt} \quad (2)$$

$$W \frac{dC_O}{dt} = \frac{M_O}{M_C} \left( W_{CO} \times \frac{dC_{CO}}{dt} + W_{Ar} \times \frac{dC_{Ar}}{dt} + W_{Splash} \times \frac{dC_{Splash}}{dt} \right) \quad (3)$$

where  $t$  is the iteration length, s;  $C_C$ ,  $C_O$  are the carbon and oxygen concentrations, respectively;  $\frac{dC_{CO}}{dt}$ ,  $\frac{dC_{Ar}}{dt}$ ,  $\frac{dC_{Splash}}{dt}$  are the decarburization rates (concentration) of CO bubbles, Ar bubbles, and splash droplets, respectively,  $s^{-1}$ ;  $W_{CO}$ ,  $W_{Ar}$ ,  $W_{Splash}$  are masses of steel in the decarburization mechanisms of CO bubbles, Ar bubbles, and splash droplets, respectively, kg;  $W$  is the mass of steel in the ladle, kg; and  $M_C$ ,  $M_O$  are molecular weights of C and O, respectively, (g/mol).

### 2.3 Decarburization rate by different mechanisms

$$(1) \quad \frac{dC_{CO}}{dt}$$

Because the C–O reaction rate is controlled by the mass transfers of carbon and oxygen, the decarburization rate of a CO bubble is calculated using Eq. (4). The CO formation region is given by Eq. (5) [13, 18].

$$\frac{dC_{CO}}{dt} = -\alpha H_{CO} (C_C \times C_O \times K - P_{CO}^*) \quad (4)$$

$$H_{CO} = (C_C \times C_O \times K - P_{CO}^*) / (\rho g) \quad (5)$$

where the coefficient  $\alpha$  is determined by the trial-and-error method of comparing calculations with the real data;  $\rho$  is the density of molten steel, (kg/m<sup>3</sup>); and  $g$  is the acceleration of gravity.

$$(2) \quad \frac{dC_{Ar}}{dt}$$

Decarburization using argon bubbles is a three-stage process of diffusion of C and O onto the bubble surface,

chemical reaction on the bubble surface, and gaseous mass transfer. The decarburization rate for the mechanism using argon bubbles is given by Eq. (6) [6, 13].

$$-\frac{dC_{Ar}}{dt} = -\frac{\frac{G}{0.0224} \times C_C \times C_O \times K}{\frac{W_{Ar}}{100M_C} (C_C \times C_O \times K - P_{CO}^*) \times 60} \quad (6)$$

where  $G$  is lift gas flow rate, (L/min).

$$(3) \quad \frac{dC_{Splash}}{dt}$$

It is supposed that all particles are round and that  $C_s$  denotes the surface C content after decarburization. The average particle size and average staying time in the vessel are assumed as 2  $\mu\text{m}$  and 2 s, respectively [20]. The decarburization of the splashing particles is then given by [13, 21, 22].

$$\frac{dC_{Splash}}{dt} = \frac{3}{4\pi R^2} \left\{ 1 - \frac{6}{\pi^2} \sum_{n=1}^{\infty} \frac{1}{n^2} \exp\left(-\frac{n^2 \pi^2 D_{Splash} \theta}{R^2}\right) \right\} (C_C - C_s) \quad (7)$$

where  $D_{Splash}$  is the average diameter of splash droplets, mm;  $\theta$  is the average staying time of splash droplets in the vacuum vessel, s; and  $R$  is the constant of 8.314 J/(K mol).

### 2.4 Weight of molten steel in different reactions

$$(1) \quad W_{CO}$$

In this model, the amount of molten steel partaking in the decarburization reaction through CO bubbling equals the weight change per second in the vacuum vessel, which equals the recirculation flow rate. The recirculation flow rate, which is often expressed by  $Q$  (kg/s), is an essential parameter in the RH refining process because circulation flow plays a crucial role in decarburization [23]. The circulation flow rate is mainly affected by the snorkel diameter and the flow rate of the lift gas. Kuwabara et al. [24] also considered the effect of pressure on  $Q$ . Their equation, which is now widely used, is adopted in the present study and is reproduced as Eq. (8)

$$Q = \frac{11,400 \times G^{1/3} \times D^{4/3} \times [\ln(P_{Atm}/P_{Vacuum})]^{1/3}}{60} \quad (8)$$

where  $G$  is the flow rate of the lifting gas, (L/min);  $D$  is the inner diameter of the up-snorkel, m;  $P_{Atm}$  is the atmospheric pressure, which is 101,325 Pa; and  $P_{Vacuum}$  is the vacuum pressure, Pa. The total weight of the C–O decarburization reaction per unit time is calculated using Eq. (9).

$$W_{CO} = \frac{11,400 \times G^{1/3} \times D^{4/3} \times [\ln(P_{Atm}/P_{Vacuum})]^{1/3}}{60} \times t \quad (9)$$

$$(2) \quad W_{Ar}$$

Li et al. [16] calculated the volume of the two-phase gas–liquid region using Eq. (10). As shown in Fig. 1, this volume is directly related to the pressure in the vacuum and the flow rate of the blow argon, which influence the internal decarburization behavior of molten steel. Under constant vacuum pressure, the gas volume of the two-phase gas–liquid region increases with increasing the blow-argon flow rate. The weight of steel in this reaction is computed using Eq. (11).

$$V_{Ar} = \frac{g(\rho - \rho_{Ar}) \times 10^3 \times G_m^2}{g(\rho - \rho_{Ar}) \times 10^3 \times G_m^2 - 0.37QRT \times \ln(P_{Atm}/P_{Vacuum})} \quad (10)$$

$$W_{Ar} = \rho \times V_{Ar} \quad (11)$$

where  $\rho_{Ar}$  is the density of Ar gas, (kg/m<sup>3</sup>);  $G_m$  is the volume of Ar bubbles, m<sup>3</sup>; and  $V_{Ar}$  is the volume of molten steel containing argon bubbles, m<sup>3</sup>.

$$(3) \quad W_{Splash}$$

Splash droplets are produced by stirring of the uplifted gas and pressure difference. Their weight increases when oxygen blows through the top oxygen lance. Chen et al. [22] empirically derived Eq. (12) via a water model experiment and revised it in an actual production process. The equation states that in a natural decarburization process, the molten steel produces splash droplets at the rate of 0.0342%/min.

$$W_{Splash} = \frac{0.000342 \times W_{Vacuum} \times t}{60} \quad (12)$$

In the initial smelting stage, the vacuum vessel pressure exceeds 29,811 Pa and molten steel has not yet entered the vacuum vessel through the snorkel tube. At this time, the volume of molten steel in the snorkel tube,  $W_{Vacuum}$ , is calculated using Eq. (13).

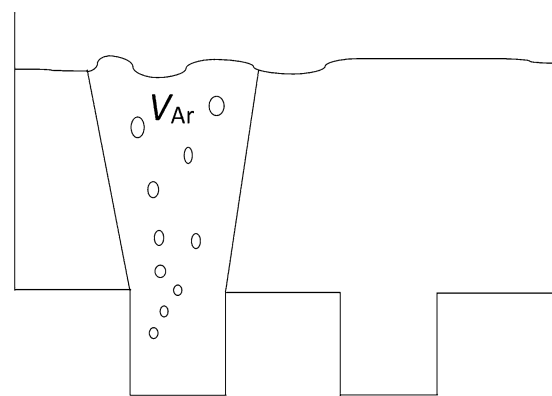


Fig. 1 Volume of two-phase region

$$W_{\text{vacuum}} = \pi \times r_1^2 \times (P_{\text{Atm}} - P_{\text{vacuum}})/g \quad (13)$$

where  $r_1$  is the radius of snorkel tube, m.

When the pressure falls below 29,811 Pa, molten steel begins to enter the vacuum vessel.  $W_{\text{vacuum}}$  now equals the summed weights of the steel in the snorkel tube and the steel in vacuum vessel:

$$W_{\text{vacuum}} = \pi \times r_1^2 \times (P_{\text{Atm}} - P_{\text{vacuum}})/g + \rho \times \pi \times r_2^2 \times [(P_{\text{Atm}} - P_{\text{vacuum}})/(\rho g) - 0.934] \quad (14)$$

where  $r_2$  is the radius of vacuum vessel, m.

## 2.5 Oxygen decarburization

When employing the oxygen lance, the smelting process is equivalent to increasing the oxygen content of the molten steel. This scenario affects only Eq. (3). (The other equations remain unchanged.) Equation (3) now becomes

$$W \frac{dC_{\text{O}}}{dt} = -\frac{M_{\text{O}}}{M_{\text{C}}} \left( W_{\text{CO}} \times \frac{dC_{\text{CO}}}{dt} + W_{\text{Ar}} \times \frac{dC_{\text{Ar}}}{dt} + W_{\text{Splash}} \times \frac{dC_{\text{Splash}}}{dt} \right) + 1429\beta F_{\text{O}_2} \quad (15)$$

where  $\beta$  is the absorption efficiency of oxygen and solved by Eq. (16);  $F_{\text{O}_2}$  is the oxygen flow rate, ( $\text{m}^3/\text{s}$ ); and  $O_{\text{in}}$  is the incoming oxygen that goes into molten steel.

$$O_{\text{in}} = 1.429 \times 10^{-3} \times \beta \times F_{\text{O}_2} \times t \quad (16)$$

According to production experience, approximately  $100 \times 10^{-6} \text{ m}^3$  of every  $20 \text{ m}^3$  of oxygen blown into the vessel is diverted into the molten steel. Therefore, the molten steel expands by  $5 \times 10^{-6} \text{ m}^3$  for every cubic meter of oxygen entering the vessel. Given the diameter of the vacuum vessel (1.8 m) and the capacity of the ladle (130 t),  $\beta$  can be calculated using Eq. (17). The calculation yields  $\beta = 45.48\%$ .

$$1.429 \times 10^{-3} \times \beta \times F_{\text{O}_2} \times t = 130 \times 5 \times 10^{-6} \times F_{\text{O}_2} \times t \quad (17)$$

## 3 Results and discussion

### 3.1 Industrial experiment

To validate the accuracy of the proposed model, an industrial experiment at S.D. STEEL (Shandong, China) was conducted. At this steel mill, the production process of ultralow carbon steel is designated as “BOF-RH-CC,” and the RH parameters used in the production process are listed in Table 1.

**Table 1** RH parameters

Parameter	Value
Volume of ladle	130 t
Diameter of vacuum vessel	1.8 m
Diameter of snorkel tube	0.48 m
Length of snorkel tube	1.435 m
Inserting depth	0.5 m
Lifting gas rate	120 $\text{m}^3/\text{h}$
Vacuum capacity	1.1 Mt/a

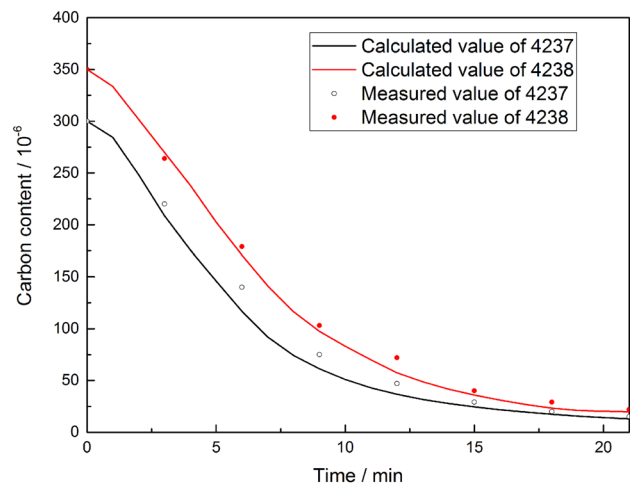


**Fig. 2** Comparison of calculated and measured carbon contents in stainless steel during a smelting process

A comparison of the measured values with the values calculated by the proposed model is shown in Fig. 2. In the industrial experiment, 4237 (short for heat H144-4237) and 4238 (short for heat H144-4238) were the heat number. During the smelting process, samples were collected every 3 min (3, 6, 9, 12, 15, 18, and 21 min) and their carbon contents were measured using a carbon–sulfur infrared analyzer. The calculation error of this model is sufficiently small to meet the requirements of engineering applications. Other verification results for the proposed model are listed in Table 2.

### 3.2 Influence of initial carbon and oxygen on decarburization

The carbon and oxygen contents at the RH station directly affect the decarburization rate and carbon content at the end point. High oxygen and low carbon contents facilitate rapid decarburization but likely cause overblowing in the basic oxygen furnace (BOF) process. If the oxygen content is excessively high in the final stages, it requires removal using large amounts of aluminum. This not only wastes valuable resources but also risks contamination of the steel

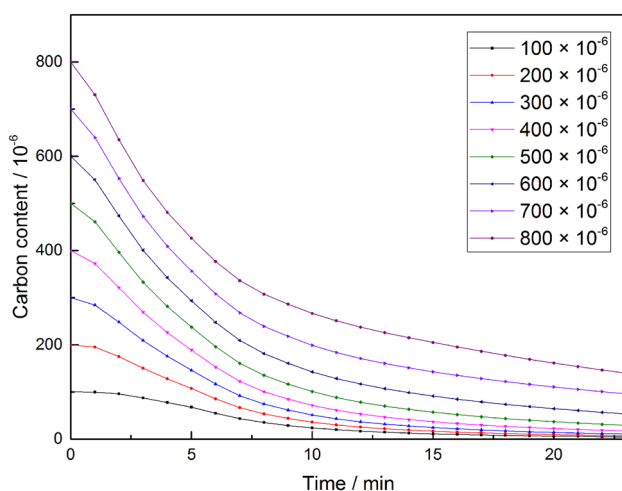
**Table 2** Other verification results for the proposed model

Number	Final time/min	Measured final carbon content/ $10^{-6}$	Calculated final carbon content/ $10^{-6}$	Deviation/ $10^{-6}$
2-1973	24	13	11	2
4-1915	23	15	10	5
2-2105	23	19	14	5
4-2285	24	15	12	3

by excess  $\text{Al}_2\text{O}_3$ . Therefore, for efficient RH decarburization, the oxygen and carbon contents at the RH station should be controlled within a reasonable range [25–27].

To study the effects of carbon content on the decarburization process, the pressure and argon data of heat 4237 and a constant oxygen content ( $800 \times 10^{-6}$ ) were used in the calculation. The time dynamics of the carbon content were then calculated for initial carbon contents ranging from  $100 \times 10^{-6}$  to  $800 \times 10^{-6}$ . The results are shown in Fig. 3.

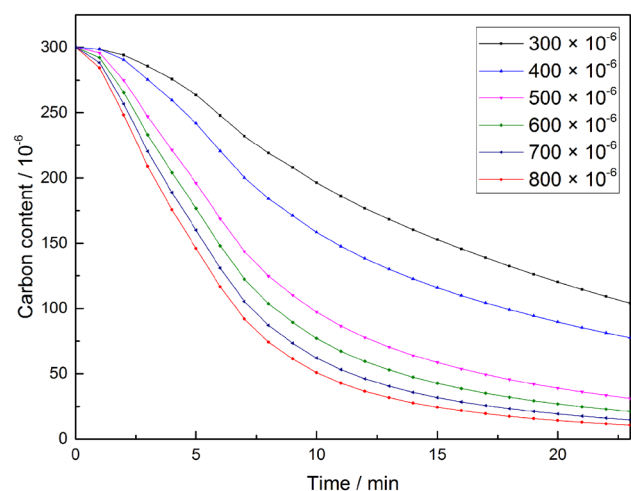
As shown in Fig. 3, increasing the initial carbon content increases the carbon content at the end of the decarburization, and when the initial carbon content is  $500 \times 10^{-6}$ , the final carbon content is much higher, which is ( $400 \times 10^{-6}$ ). Thus, when the oxygen content is  $800 \times 10^{-6}$ ,  $400 \times 10^{-6}$  is the critical value and decreasing the initial carbon content below the critical value enables rapid decarburization. However, if the initial carbon content is too low, an additional burden is imposed on the converter, which hampers the production efficiency. Therefore, to maintain an appropriate decarburization time, the initial carbon content should be controlled in the range of  $(200\text{--}350) \times 10^{-6}$ . A high initial carbon content should also achieve rapid decarburization when the top gun in the RH equipment is used to accelerate the decarburization process when the initial carbon content is higher than

**Fig. 3** Influence of initial carbon content on decarburization

$400 \times 10^{-6}$ . However, the boundary between natural decarburization and KTB (KAWASAKI top blowing) depends on the oxygen content as well as the condition of the equipment. If the oxygen content is changed, the critical value would change with it. Therefore, the boundary between natural decarburization and KTB is not a fixed value.

The effects of oxygen content on the decarburization process were investigated. The pressure and argon data of heat 4237 and a constant initial carbon content ( $300 \times 10^{-6}$ ) were used in this calculation. The time dynamics of the carbon content were then calculated for oxygen content ranging of  $(300\text{--}800) \times 10^{-6}$ . The results are shown in Fig. 4.

As shown in Fig. 4, a high initial oxygen content reduced the carbon content at the end of the decarburization process. This is attributable to the rapid decay of the curve (indicating an elevated decarburization rate). Although the initial oxygen content above  $700 \times 10^{-6}$  had negligible impact on the final carbon content, the high oxygen content at the end increased aluminum consumption. When the initial oxygen content is below  $400 \times 10^{-6}$ , carbon removal from the steel is excessively slow. Therefore, for the initial carbon content of  $300 \times 10^{-6}$ , there is also a critical oxygen content (about  $500 \times 10^{-6}$ ) that maximizes the decarburization rate. If the initial oxygen

**Fig. 4** Influence of initial oxygen content on decarburization



content in the steel is below the critical value, the decarburization rate is low and the oxygen supply must be boosted using the top gun. This process is called the *forced decarburization process*. Conversely, if the initial oxygen content exceeds the critical value, the target carbon content can be achieved using the natural decarburization process. Although increasing the initial oxygen content decreases the final carbon content, excessively high initial oxygen content is undesirable, because increasing the initial oxygen content to higher levels induces only a small effect and it may raise the oxygen content to unacceptably high levels.

The above analysis confirms that stable initial oxygen and carbon contents are essential in the RH decarburization processes. At S.D. STEEL, the stable content ranges are  $(500\text{--}700) \times 10^{-6}$  for oxygen and  $(200\text{--}350) \times 10^{-6}$  for carbon.

### 3.3 Influence of vacuum pressure on decarburization

After oxidization, the carbon in molten steel forms CO bubbles; therefore, reducing the partial pressure of CO will accelerate the decarburization reaction and lower the C–O equilibrium value. Therefore, an RH degasser with a vacuum vessel is widely used in the production of ultralow carbon steel [28].

As the falling rate of pressure in the vacuum is high, the rate of the decarburization reaction increases and the final carbon content reduces [5–19]. A high vacuum degree will hasten the growth rate and the rising speed of the CO bubbles. Therefore, the CO bubbles more rapidly depart from the gas–liquid boundary to the gas phase, thereby accelerating the decarburization rate [28]. To study the effect of the pressure reduction rate on the decarburization, the pressure-decrease rate was slowed down to compare with the data obtained from heat 4237 (Fig. 5). In Fig. 6, two initial data groups,  $(300, 800) \times 10^6$  and  $(400, 600) \times 10^6$ , were selected from the data of heat 4237. The  $(300, 800) \times 10^6$  group represents low initial carbon and high initial oxygen contents; the  $(400, 600) \times 10^6$  group represents high initial carbon and low initial oxygen contents. The decarburization curves of both groups under different vacuum conditions are shown in Fig. 6.

Under both sets of initial conditions, i.e.,  $(300, 800)$  and  $(400, 600)$ , a faster pressure-reducing rate yielded a better decarburization result than the slow pressure-reducing rate process. For example, if the end point of the decarburization was set to  $20 \times 10^{-6}$ , the heat 4237 requires 17 min, which is 5 min less than the time taken by the slow pressure-reducing rate process. Therefore, a rapid reduction in pressure is beneficial to the decarburization process.

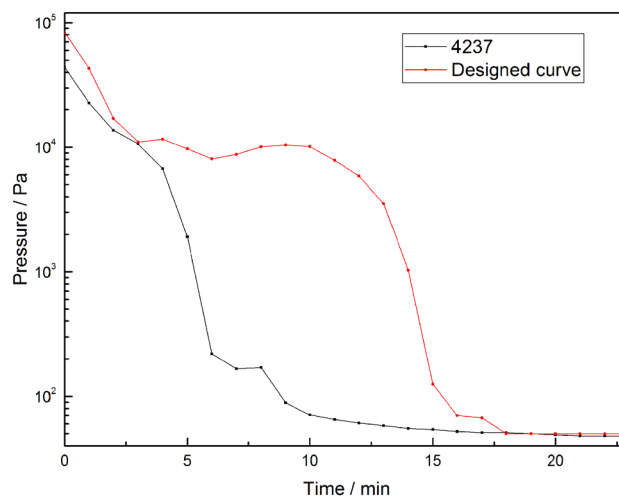


Fig. 5 Pressure of heat 4237 and designed curve

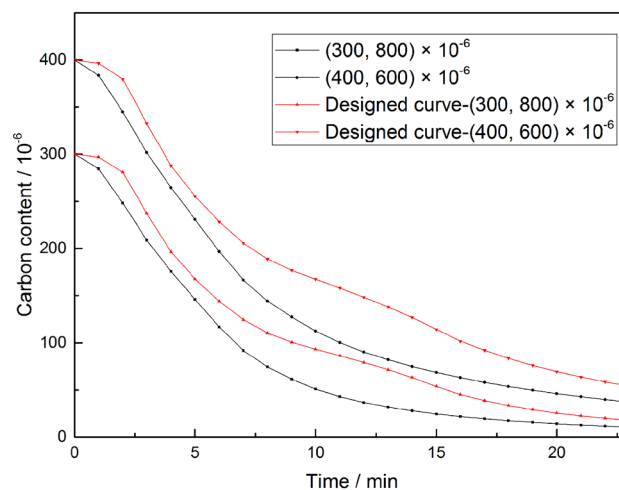


Fig. 6 Influence of vacuum pressure on decarburization

### 3.4 Influence of snorkel tube diameter on decarburization

Generally, the recirculation flow rate increases with snorkel diameter and is also significantly affected by the decarburization rate [29]. The relationship between the snorkel diameter, recirculation flow rate, and decarburization rate has been extensively reported by previous studies [23, 30]. Table 3 lists the maximum recirculation flow rates under the current argon-blowing process at S.D. STEEL. Here, the snorkel tube diameter varied from 480 mm to 840 mm, and the flow rates were calculated using Eq. (8). As the diameter increased from 480 mm (the current working condition) to 600 mm, the recirculation flow rate increased from 101.8 to 137.1 t/min, which is an increase of 38%.

The data obtained from heat 4237 are selected, and the initial carbon and oxygen contents are set to  $300 \times 10^{-6}$

**Table 3** Maximum flow rates for different snorkel tube diameters

Diameter/mm	240	360	480	600	720	840
Value/(t min <sup>-1</sup> )	41.0	70.4	101.8	137.1	174.8	214.0

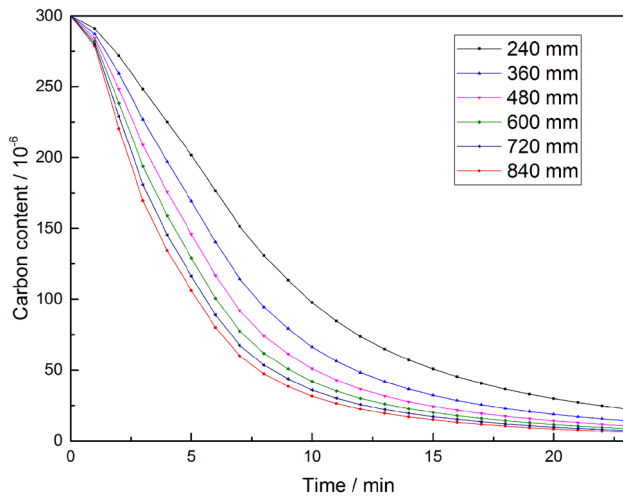


**Fig. 7** Influence of snorkel tube diameter on decarburization

and  $800 \times 10^{-6}$ , respectively. To study the influence of snorkel diameter on the decarburization rate, different snorkel diameters used for calculation are listed in Table 3. The results are plotted in Fig. 7. The decarburization rate is a gradually increasing function of snorkel diameter. The increase in snorkel diameter from 240 mm to 600 mm exhibits the most significant effect on the decarburization rate; however, above 600 mm, the effects are less obvious. Moreover, the effects of snorkel diameter are most evident in the early decarburization stages and they reduce at later stages. Therefore, increasing the snorkel diameter improves the removal efficiency, hastens decarburization, and shortens the melting time. As shown in Fig. 7, raising the snorkel diameter from 400 mm to 600 mm reduces the refining time by approximately 2 min.

### 3.5 Influence of oxygen-blowing process on decarburization

The production process of ultralow carbon steel can be effectively improved by blowing oxygen into steel through the water-cooled oxygen lance located at the top of the vacuum vessel [16, 18]. Under initial conditions of high carbon and low oxygen contents, the oxygen mass transfer to the reaction interface often becomes the limiting step in decarburization. The oxygen lance rapidly increases the

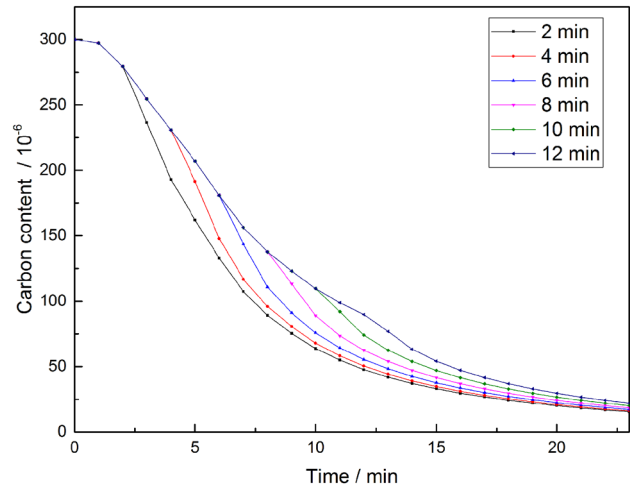


**Fig. 8** Influence of blowing start time on decarburization

oxygen content of the liquid steel in the vacuum vessel. The oxygen supply increases the mass transfer rate of oxygen on the surface of the argon gas bubbles and the liquid droplets in the vacuum vessel while increasing the depth of the CO bubbles produced by the C–O reaction. Both mechanisms accelerate the entire decarburization process [9].

The oxygen flow at S.D. STEEL is  $1500 \text{ m}^3/\text{h}$ , namely  $25 \text{ m}^3/\text{min}$ . To study the effect of the oxygen decarburization start time, the initial carbon and oxygen contents are set as  $300 \times 10^{-6}$  and  $400 \times 10^{-6}$ , respectively, and the oxygen-blowing time to 120 s (admitting  $50 \text{ m}^3 \text{ O}_2$ ). The carbon content dynamics for different start time are plotted in Fig. 8. Figure 8 confirms that the earlier the start time, the higher the decarburization speed. Therefore, to improve the removal efficiency of carbon, the oxygen blowing should be applied as early as possible.

The flow rate of the oxygen supply may also affect the removal efficiency. Currently, the flow rate in the steel mill is  $1500 \text{ m}^3/\text{h}$  (or  $0.1923 \text{ m}^3/(\text{t min})$ ). To study the effect of this flow rate on the decarburization process, the initial (oxygen, carbon) value is set as (300, 400), and blowing started in  $50 \text{ m}^3$  oxygen. Five minutes later, the decarburization treatment is started and the carbon and oxygen contents under different oxygen flow rates (0.0641, 0.1282, 0.1923, 0.2564, and  $0.3205 \text{ m}^3/(\text{t min})$ ) are calculated. The effects of oxygen flow rate on carbon content are plotted in Fig. 9. The decarburization rate is affected only at the lowest flow rate ( $0.0641 \text{ m}^3/(\text{t min})$ ). Above a critical value, the oxygen flow rate negligibly affects the decarburization rate. Therefore, for achieving the best decarburization performance, the critical flow rate should be selected, i.e.,  $0.1923 \text{ m}^3/(\text{t min})$  (shown in Fig. 9).

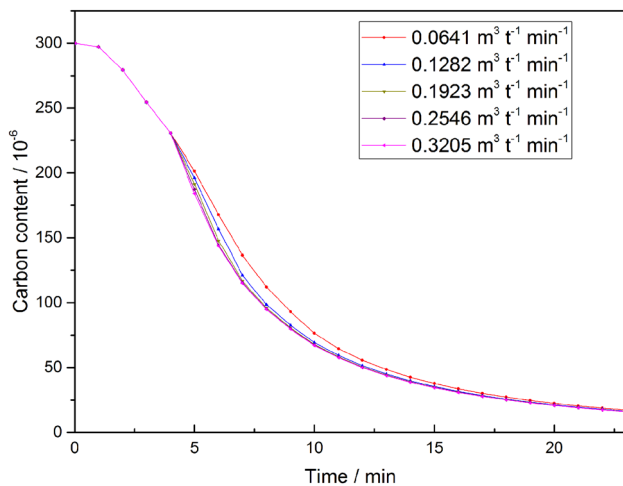


Fig. 9 Influence of oxygen flow rate on decarburization

## 4 Conclusions

1. For the 130 t RH degasser, the initial carbon content should be stabilized within the range of  $(200\text{--}350) \times 10^{-6}$ ; the ideal initial oxygen content is  $(500\text{--}700) \times 10^{-6}$ , and the pressure should be reduced as quickly as possible in the early stage of decarburization.
2. Oxygen blowing should begin as early as possible when the forced decarburization is needed in the decarburization process, and the oxygen flow rate should not be less than  $0.1923 \text{ m}^3/(\text{t min})$  for the 130 t RH degasser.
3. For the 130 t RH degasser, expanding the diameter of the snorkel tube from 480 to 600 mm can reduce the refining time by approximately 2 min.

**Acknowledgements** The authors would like to acknowledge the National Natural Science Foundation of China (51574063), Fundamental Research Funds for the Central Universities (N150204012, N152306001), and Program for Liaoning Excellent Talents in University (LJQ2015056).

## References

- [1] X.G. Ai, C.S. Wang, F.T. Meng, S.L. Li, H.X. Liu, Y. Gan, J. Iron Steel Res. 28 (2016) No. 1, 20–24.

- [2] K. Feng, D.F. He, A.J. Xu, H.B. Wang, J. Iron Steel Res. Int. 22 (2015) No. S1, 68–74.
- [3] Y.N. Wang, Y.P. Bao, H. Cui, B. Chen, C.X. Ji, J. Iron and Steel Res. Int. 19 (2012) No. 3, 1–5.
- [4] C.F. Lv, D.L. Shang, L. Kang, W.W. Zhang, G.H. Chang, J. Iron Steel Res. 26 (2014) No. 6, 11–16.
- [5] K. Yamaguchi, Y. Kishimoto, T. Sakuraya, T. Fujii, M. Aratani, H. Nishikawa, ISIJ Int. 32 (1992) 126–135.
- [6] M. Takahashi, H. Matsumoto, T. Saito, ISIJ Int. 35 (1995) 1452–1458.
- [7] B. Deo, S. Gupta, Steel Res. Int. 67 (1996) 7–11.
- [8] Y. Higuchi, H. Ikenaga, Y. Shirota, Tetsu-to-Hagane. 84 (1998) 709–714.
- [9] H. Saint-Raymond, D. Huin, F. Stouvenot, Mater. Trans. JIM 41 (2000) 17–21.
- [10] M.Y. Zhu, Z.Z. Huang, Acta Metall. Sin. 37 (2001) 91–94.
- [11] Y.G. Park, K.W. Yi, ISIJ Int. 43 (2003) 1403–1409.
- [12] X.D. Yin, Z.Z. Huang, W.B. Gu, Acta Metall. Sin. 41 (2005) 876–880.
- [13] C.J. Han, L.Q. Ai, B.S. Liu, J. Zhang, Y.P. Bao, K.K. Cai, J. Univ. Sci. Technol. Beijing 13 (2006) 218–221.
- [14] B.S. Liu, G.S. Zhu, H.X. Li, B.H. Li, Y. Cui, A.M. Cui, Int. J. Miner. Metall. Mater. 17 (2010) 22–27.
- [15] M.A. Van Ende, Y.M. Kim, M.K. Cho, J. Choi, I.H. Jung, Metall. Mater. Trans. B 42 (2011) 477–489.
- [16] C.W. Li, G.G. Cheng, X.H. Wang, G.S. Zhu, A.M. Cui, J. Iron Steel Res. Int. 19 (2012) No. 5, 23–29.
- [17] J.M. Zhang, L. Liu, X.Y. Zhao, S.W. Lei, Q.P. Dong, ISIJ Int. 54 (2014) 1560–1569.
- [18] P.H. Li, Q.J. Wu, W.H. Hu, J.S. Ye, J. Iron Steel Res. Int. 22 (2015) No. S1, 63–67.
- [19] D.Q. Geng, J.X. Zheng, K. Wang, P. Wang, R.Q. Liang, H.T. Liu, H. Lei, J.C. He, Metall. Mater. Trans. B 46 (2015) 1484–1493.
- [20] J.X. Chen, Common chart and data for steelmaking, 2nd edition, Metallurgical Industry Press, Beijing, 2010.
- [21] J.H. Wei, Journal of Shanghai University 7 (2003) 97–117.
- [22] Y.S. Chen, Y.D. He, Z.Z. Huang, Journal of Inner Mongolia University of Science and Technology 26 (2007) 1–5.
- [23] O. Nakamura, M. Numata, K. Takatani, Tetsu-to-Hagane 101 (2015) 123–128.
- [24] T. Kuwabara, K. Umezawa, K. Mori, H. Watanabe, Trans. ISIJ 28 (1988) 305–314.
- [25] Y.H. Li, Y.P. Bao, M. Wang, R. Wang, D.C. Tang, Ironmak. Steelmak. 42 (2015) 366–372.
- [26] M. Wang, Y.P. Bao, Q. Yang, L.H. Zhao, L. Lin, Int. J. Miner. Metall. Mater. 22 (2015) 1252–1259.
- [27] M. Wang, Y.P. Bao, L.H. Zhao, Q. Yang, L. Lin, ISIJ Int. 55 (2015) 1652–1660.
- [28] R. Ding, B. Blanpain, P.T. Jones, P. Wollants, Metall. Mater. Trans. B 31 (2000) 197–206.
- [29] F. Jiang, G.G. Cheng, Ironmak. Steelmak. 39 (2012) 386–390.
- [30] D.Q. Geng, H. Lei, J.C. He, ISIJ Int. 52 (2012) 1036–1044.